AIP | Journal of Applied Physics

Investigation of the pressure dependent thermodynamic and elastic properties of 1,3,5-triamino-2,4,6-trinitrobenzene using dispersion corrected density functional theory

A. A. Rykounov

Citation: Journal of Applied Physics **117**, 215901 (2015); doi: 10.1063/1.4921815
View online: http://dx.doi.org/10.1063/1.4921815
View Table of Contents: http://scitation.aip.org/content/aip/journal/jap/117/21?ver=pdfcov
Published by the AIP Publishing

Investigation of the pressure dependent thermodynamic and elastic properties of 1,3,5-triamino-2,4,6-trinitrobenzene using dispersion corrected density functional theory

A. A. Rykounov
Russian Federal Nuclear Center – All-Russian Research Institute of Technical Physics (RFNC-VNIITF), Snezhinsk, Chelyabinsk Region, Russia

(Received 21 December 2014; accepted 17 May 2015; published online 1 June 2015)

The influence of pressure on the thermodynamic, structural, and elastic properties of the 1,3,5-triamino-2,4,6-trinitrobenzene (TATB) molecular crystal at T = 0 is systematically studied. Calculations are carried out using density functional theory methods in a plane wave basis set with dispersion corrections for the exchange-correlation part of total energy, and ultrasoft pseudopotentials. The equilibrium unit cell parameters, the cold compression curve in the pressure range of 0–50 GPa and the sound speeds are computed. The effect of finite pressure on the molecular structure of TATB is elucidated from the analysis of relative changes in the intra- and intermolecular geometrical parameters. For the first time, the full set of elastic constants of this crystal at zero and non-zero pressures is determined from *ab initio* calculations. The resulted structural, elastic, and acoustic properties of TATB are shown to be in a good agreement with available experimental and theoretical data. © *2015 AIP Publishing LLC*. [http://dx.doi.org/10.1063/1.4921815]

I. INTRODUCTION

Practical interest to the study of the 1,3,5-triamino-2,4,6-trinitrobenzene (TATB) structure both by experimental and by theoretical methods is primarily determined by a unique combination of the detonating properties of this compound: low sensitivity to heat, and electrical and shock impacts together with the relatively high detonation pressure and velocity. In addition, the nonlinear optical activity of TATB crystal[1–3] deserves consideration because it does not fully agree with the experimentally determined centrosymmetrical space group.[4] The wide use of TATB and TATB-based formulations (such as PBX 9502) in practice determines the interest to the theoretical investigation of the TATB structure and its modification due to external factors, for example, pressure and temperature.

TATB crystallizes in a triclinic unit cell with the $P\bar{1}$ space symmetry group containing two molecules (Fig. 1). The intermolecular interaction types significantly differ along the crystallographic axes. Molecules are arranged in planar hydrogen-bonded graphite-like sheets parallel to the *a-b* plane. On the other hand, along the *c* axis molecules are bonded only by the weak van der Waals forces. The equilibrium cell parameters at ambient conditions were measured by Cady and Larson[4] in 1965, and since that, as far as we know, no X-ray diffraction studies have been published for TATB monocrystal.

The quantitatively correct equilibrium cell parameters for TATB can hardly be determined within the classical DFT approaches because of the known difficulties with accounting for dispersion interactions[5] in standard GGA and hybrid functionals. This is confirmed by the early works devoted to the determination of TATB equilibrium cell parameters using both local density approximation and generalized gradient approximation exchange-correlation functionals (see Ref. 6, for example, where PW91[7] and PBE[8] functionals were used).

This work is aimed to investigate the effects of finite pressure on the thermodynamic, elastic, and acoustic properties of TATB as well as on its molecular structure at zero temperature using the DFT-D2 dispersion corrections by Grimme.[9] The choice of this type of corrections was determined by four factors. First, the theoretical foundations of this approach stemming from the multipole-multipole interaction model are clear and simple. Second, the efficiency of Grimme corrections for the prediction of the equilibrium properties of energetic materials including TATB was shown by other researchers.[10–14] Third, the DFT-D2 correction is included in a number of freely available program packages such as Quantum ESPRESSO[15] used in this work. Fourth, the inclusion of this correction has only a minor influence on the total time of calculation.

After determining the optimal calculation parameters, we discuss the cold compression curve in the context of cell parameters and the pressure influence on the structural characteristics of the TATB molecule. Then, we describe calculations for elastic constants and sound speeds at different pressures.

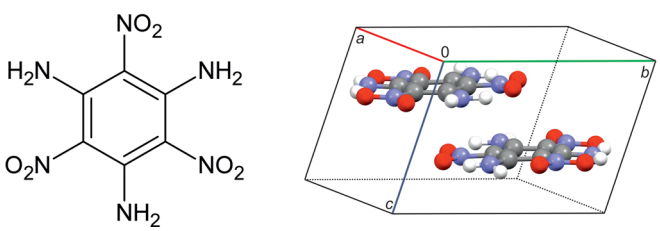

FIG. 1. The structural formula and the unit cell of TATB crystal. Carbon, nitrogen, oxygen, and hydrogen atoms are colored gray, blue, red, and white, respectively.

II. STRUCTURAL AND THERMODYNAMIC PROPERTIES

A. Determination of optimal calculation parameters

The calculation of elastic constants which are essentially the second derivative of total energy with respect to strain requires a serious preliminary consideration of optimal calculation parameters. The additional difficulty is that TATB, like other energetic materials (see, for example, the recent work by Taylor[16]), is a relatively "soft" material with elastic constants about a few GPa at zero pressure. It means that finding a minimum on the potential energy surface is quite complicated for such systems. Therefore, the system under study should be at least tested for convergence in the basis set and *k*-points sampling.

All calculations described in this work were performed with the Quantum ESPRESSO[15] program package in the plane wave basis set with ultrasoft (US) Vanderbilt pseudopotentials[17] parameterized for the PBE[8] functional. We also tested the performance of the norm-conserving pseudopotentials in the form of Troullier-Martins[18,19] (TM) with and without dispersion correction.

Using originless plane waves as basis functions delivers us from the basis set superposition error[20,21] unlike spatially localized Gaussian functions, which makes the calculation of energy differences very accurate if the same box size and number of plane waves are used.[22] The plane wave cutoff determining the basis set size was tested from 60 to 100 Ry for the TM pseudopotentials and from 40 to 100 Ry for the US pseudopotentials. The convergence of total energy on the level 0.1 mRy/atom was achieved at 60 Ry (816 eV) for the US pseudopotentials and at 80 Ry (1088 eV) for the norm-conserving pseudopotentials at zero pressure. It is worth to note that this level of theory is quite high and not achieved in the majority of papers dealing with molecular crystals. However, such a level is needed for the detection of small changes in energy in the calculations of elastic properties.

We also tested the performance of ultrasoft pseudopotentials for the compressed structure at pressure 50 GPa and obtained that the cell structural parameters and total energy remained essentially the same above the cutoff energy 40 Ry. Moreover, the total time of calculation for high pressures was much lower than that for zero pressure because a smaller number of iterations were needed to reach convergence in the total energy and its gradient. This observation probably reflects the "sharpening" of the potential energy surface minimum with the pressure growing.

Another way to "improve" the theoretical level of calculation is to make the *k*-points grid denser in reciprocal space. It should be noted that usually in calculations of organic compounds having closed electronic shells researchers limit themselves to the Γ-point only. We also performed such calculations and convinced that the only *k*-point is insufficient to reproduce the experimental data for any type of pseudopotentials used in the case of TATB. We then tested some symmetrical *k*-points grid with sizes $2\times2\times2$ (8 *k*-points in the irreducible Brillouin zone), $3\times3\times3$ (14 *k*-points), $4\times4\times4$ (36 *k*-points), and $5\times5\times5$ (63 *k*-points); and some non-symmetrical grids $3\times3\times2$ (10 *k*-points), $6\times6\times4$ (76 *k*-points), and $9\times9\times6$ (244 *k*-points). The accuracy of the cell vectors on the level ±0.001 Å and the cell angles on the level 0.01° is already achieved with the smallest *k*-points grid of size $2\times2\times2$.

For all calculations presented below, we use the cutoff energy of 100 Ry and the $3\times3\times2$ grid of *k*-points. The equilibrium cell parameters obtained on this level of theory are compared with the experimental data of Cady and Larson in Table I. We suppose that the selected theoretical level is sufficient for calculating the chosen characteristics as functions of total energy and its derivatives. As follows from Table I, the cell vector lengths are accurate within 4%, the angles are within 1%, and the cell volume is within 3%. As expected, the largest deviations are obtained for the parameters *c* and α which are related to the interlayer packing and orientation. From Table I, it can be seen that the cell volume obtained on the same level of theory using both ultrasoft and TM pseudopotentials *without* dispersion corrections is unbelievably large, and all lattice parameters, especially the length of the vector *c* and the value of the angel α, are considerably deviated from the corresponding experimentally measured values. Therefore, the use of dispersion corrections for a proper description of the equilibrium lattice parameters of TATB is mandatory.

B. Cold compression curve

The unit cell parameters and corresponding densities along the isotherm $T=0$ are calculated for pressures up to 50 GPa and presented in Table II. So far, as experimental data for the relative volume of compressed TATB are available only up to 13.0 GPa, in Fig. 2 we show the calculated points for the pressure range of 0–15 GPa together with experimental hydrostatic compression data by Stevens[23] and by Olinger and Cady.[24] The agreement of our data with the experimental datasets is very good with the exception of one point of Ref. 24 for the largest pressure. It should be pointed out that Olinger and Cady make some assumptions about the compression behavior of TATB to reduce the number of the X-ray spectrum peaks needed for deducing the unit cell parameters. Therefore, the uncertainty of their data at higher

TABLE I. Equilibrium cell parameters of TATB obtained with TM and US pseudopotentials (the inclusion of the dispersion correction is denoted by "disp").

Cell parameter[a]	Experiment (Ref. 4)	TM	TM, disp	US	US, disp
a	9.010	9.194	9.036	9.258	9.072
b	9.028	9.209	9.051	9.258	9.089
c	6.812	7.312	6.505	7.282	6.569
α	108.59	104.42	109.77	92.09	109.57
β	91.82	90.86	92.03	89.60	91.66
γ	119.97	120.07	119.94	120.02	119.95
Cell volume	442.49	511.61	419.99	540.06	429.26
Total energy		−772.7535	−772.9776	−770.8143	−771.0350

[a]Cell parameters are given in Angstrom units and energy is in Ry/cell.

TABLE II. The calculated unit cell parameters of TATB on the cold compression curve.

Pressure (GPa)	V, Å^3	ρ, g/cm^3	V/V_0	a, Å	b, Å	c, Å	α, deg	β, deg	γ, deg
0.0	432.401	1.9827	1	9.0839	9.0987	6.5927	109.45	91.57	119.97
0.1	429.327	1.9969	0.993	9.0742	9.0896	6.5678	109.54	91.67	119.96
0.2	426.390	2.0107	0.986	9.0646	9.0803	6.5439	109.59	91.81	119.95
0.5	418.698	2.0476	0.968	9.0376	9.0567	6.4859	109.90	91.97	119.95
1.0	408.643	2.0980	0.945	9.0012	9.0216	6.4007	110.21	92.05	119.93
2.0	393.476	2.1789	0.910	8.9409	8.9614	6.2761	110.66	92.14	119.92
3.0	382.357	2.2422	0.884	8.8927	8.9133	6.1861	111.04	92.07	119.92
4.0	373.446	2.2957	0.864	8.8524	8.8722	6.1120	111.32	91.98	119.92
5.0	365.995	2.3425	0.846	8.8168	8.8360	6.0505	111.55	91.91	119.92
7.5	351.563	2.4386	0.813	8.7436	8.7640	5.9310	112.01	91.77	119.92
10.0	340.542	2.5176	0.788	8.6857	8.7055	5.8382	112.33	91.65	119.92
12.5	331.552	2.5858	0.767	8.6356	8.6551	5.7632	112.58	91.58	119.92
15.0	323.940	2.6466	0.749	8.5924	8.6124	5.6990	112.80	91.52	119.92
17.5	317.285	2.7021	0.734	8.5539	8.5742	5.6424	112.99	91.47	119.93
20.0	311.341	2.7537	0.720	8.5189	8.5391	5.5917	113.16	91.43	119.93
22.5	305.958	2.8021	0.708	8.4867	8.5071	5.5451	113.31	91.41	119.93
25.0	301.028	2.8480	0.696	8.4570	8.4771	5.5020	113.45	91.38	119.94
27.5	296.467	2.8918	0.686	8.4291	8.4492	5.4617	113.58	91.36	119.94
30.0	292.221	2.9339	0.676	8.4029	8.4229	5.4238	113.69	91.35	119.94
32.5	288.247	2.9743	0.667	8.3781	8.3979	5.3880	113.80	91.33	119.94
35.0	284.507	3.0134	0.658	8.3547	8.3741	5.3539	113.90	91.32	119.94
37.5	280.981	3.0512	0.650	8.3324	8.3515	5.3214	114.00	91.31	119.94
40.0	277.641	3.0879	0.642	8.3112	8.3298	5.2904	114.09	91.29	119.94
42.5	274.471	3.1236	0.635	8.2903	8.3094	5.2607	114.18	91.28	119.94
45.0	271.456	3.1583	0.628	8.2707	8.2894	5.2322	114.26	91.26	119.94
47.5	268.584	3.1921	0.621	8.2520	8.2702	5.2051	114.34	91.24	119.93
50.0	265.843	3.2250	0.615	8.2340	8.2516	5.1789	114.42	91.23	119.94

pressures may be quite large. In Fig. 2, the theoretical data from Ref. 6 obtained by DFT calculations without dispersion corrections are also shown. It is clear that the classical DFT approaches are unable to reproduce the compression behavior of TATB crystal. Therefore, the inclusion of dispersion corrections is absolutely necessary for a correct description of the pressure effects on the structural properties of this system.

The full cold compression curve was fit by the semi-empirical equations of state (EoS) in the form of Vinet[25]

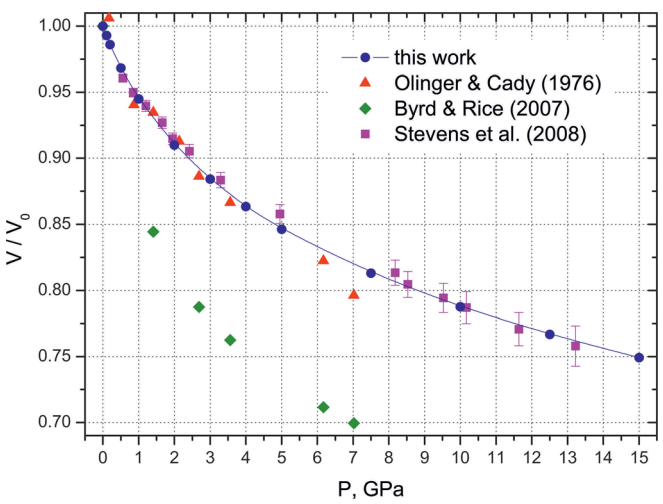

FIG. 2. Cold compression curve of TATB.

$$P = 3B\left(\frac{V}{V_0}\right)^{-2/3}\left(1-\left(\frac{V}{V_0}\right)^{1/3}\right) \times \exp\left[\frac{3}{2}(B'-1)\left(1-\left(\frac{V}{V_0}\right)^{1/3}\right)\right] \quad (1)$$

and third-order Birch-Murnaghan[26]

$$P = \frac{3}{2}B\left[\left(\frac{V}{V_0}\right)^{-7/3}-\left(\frac{V}{V_0}\right)^{-5/3}\right] \times \left[1+\frac{3}{4}(B'-4)\left(\left(\frac{V}{V_0}\right)^{-2/3}-1\right)\right], \quad (2)$$

where V_0 is the equilibrium unit cell volume. The parameters B and B' in these equations have the physical meaning of the bulk modulus and its pressure derivative, correspondingly. The approximation of data points by the Vinet equation gives $B = 18.0 \pm 0.9$ GPa, $B' = 7.74 \pm 0.24$ in comparison with $B = 16.2 \pm 4.4$ GPa, $B' = 6.1 \pm 2.8$ by Olinger and Cady; and $B = 17.5 \pm 1.8$ GPa, $B' = 7.6 \pm 0.9$ by Stevens room temperature data. The estimations using the third-order Birch-Murnaghan equation gives $B = 17.0 \pm 1.2$ GPa, $B' = 8.6 \pm 0.6$ with a somewhat larger 95% confidence interval compared with the Vinet EoS. The corresponding values from Stevens data are $B = 17.0 \pm 2.1$ GPa and $B' = 8.1 \pm 1.4$, and from the Olinger and Cady data are $B = 16.2 \pm 4.7$ GPa and $B' = 5.9 \pm 3.3$. Thus, the computed equations of states at $T = 0$ are in a good agreement with the experimental data. We will below

(Sec. III) compare the values of the bulk modulus obtained using these two EoS with the bulk modulus calculated from the elastic constants.

It is very desirable to explain the high stability of TATB as an explosive in terms of the dependence of structural molecular parameters on external factors. Therefore, it is quite natural that many works are devoted to the study of intra- and intermolecular interactions in TATB. Thus, in Ref. 27 it is proposed that TATB stabilization is achieved due to appreciable "push-pull" conjugation and the existence of a dense net of hydrogen bonds arising from interactions between nitro and amino groups. Davidson *et al.*[28] measured the Raman spectra of TATB single crystal and reported an unusually high chemical stability of samples under high static pressures. They proposed two pressure-induced subtle structural phase transitions at 28 and 56 GPa caused by changes in the interlayer hydrogen bond network due to the re-orientation of nitro groups. In contrast with their measurements, we did not observe any structural transformation of TATB crystal under compression for the entire range of pressures (0–50 GPa) studied. Pravica *et al.*[29,30] measured the IR spectra of TATB at hydrostatic pressures up to 40 GPa. They found that the peak frequencies of the NH_2 symmetric and antisymmetric vibrational modes steadily decreased with the increasing pressure, indicating the strengthening of intermolecular hydrogen bonding with pressure, but did not find any evidence of structural transitions or chemical decomposition up to the highest pressures studied as we also saw from our calculations. Manaa and Fried[31] studied the TATB crystal structure under pressures up to 250 GPa using spin-polarized density functional calculations without dispersion corrections and discovered the increasing strength of intermolecular hydrogen bonds with the growth of applied pressure. The lengths of inter- and intramolecular hydrogen bonds became equal at about 30 GPa. Ojeda and Çağin[32] showed a similar behavior of hydrogen bonds and found that the full number of interlayer hydrogen bonds increases from 0 to 8 per molecule at 1.6 GPa.

It is very interesting to evaluate the effect of finite pressures on the TATB structure in the context of relative changes in the intra- and intermolecular bond lengths using up-to-date theoretical approach. The changes of the covalent bond lengths from our dispersion corrected density functional calculations are shown in Fig. 3. All points were obtained by averaging the corresponding bond length in the molecule. The relative changes of N-H and N = O bond lengths are the smallest. This confirms that TATB compression along layers happens mostly at the expense of H-bond lengths reduction. The most compressible covalent bond in TATB is C-NO_2. Such a large reduction might lead to a considerable redistribution of electronic density and related characteristics in a compressed TATB molecule. This however needs and approval which is beyond the scope of this work but can be done in another study into the electron density dependent characteristics, for example, with use of Bader quantum topological theory.[33]

The change in the shortest intermolecular distances between pairs of atoms in adjacent layers is shown in Fig. 4. At zero pressure, when molecules in the layer are almost flat,

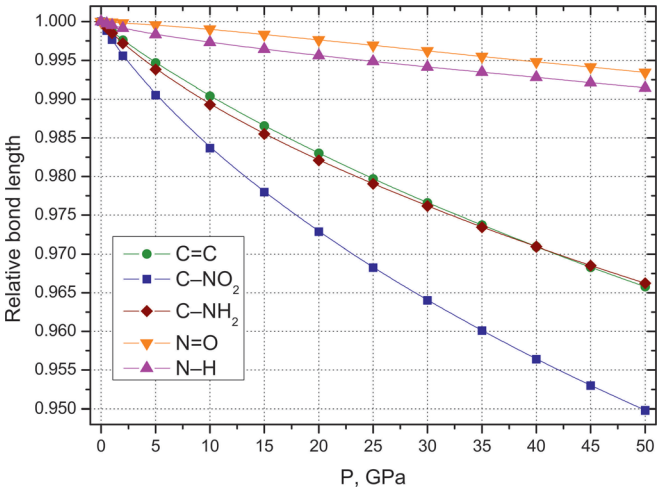

FIG. 3. Relative changes of the covalent bonds lengths under pressure.

the distances of all three types are close to each other. However, as pressure grows, the distance H···H decreases steeper than the distances N···C and H···C. It means that molecules in adjacent layers are bended towards each other. At high pressures, the TATB molecule has a form of arc in a plane perpendicular to the benzene ring. This deformation leads obviously to an additional increase of interlayer interactions at high pressures as was pointed out by other authors.[31,32]

III. ELASTIC PROPERTIES

A. Elastic constants

The correct description of the elastic properties of energetic materials is crucial for the understanding of their behavior under pressure. In particular, the determination of the full set of the second-order elastic constants (C_{ij}) allows one to describe elastic properties of a crystal, which can be used for the prediction of the sensitivity and reactivity of explosives under external mechanical stress. To the best of our knowledge, the elastic constants of the TATB

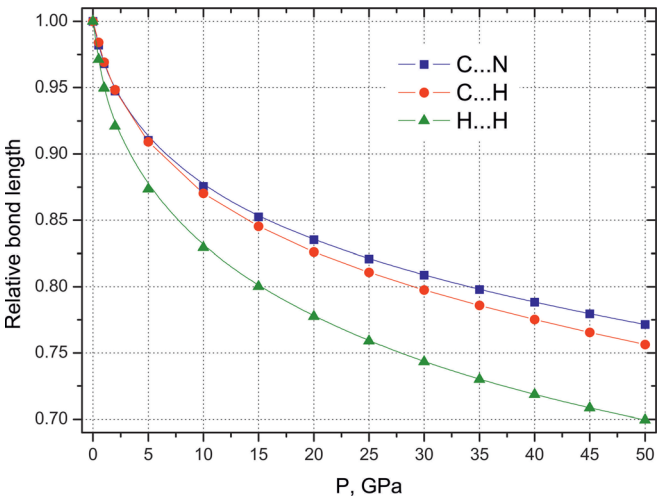

FIG. 4. The change of the shortest intermolecular distances between pairs of atoms in adjacent TATB layers with pressure.

monocrystal have not been measured experimentally. Moreover, there are only two theoretical works devoted to this issue.[13,34]

In the first work,[34] classical molecular dynamics (MD) was used to model TATB crystal with dipole polarizable and nonpolarizable force fields. Gas-phase atomic polarizabilities, partial atomic charges, and geometrical properties were parameterized using density functional theory and perturbation theory methods. As a result, the authors achieved reasonable agreement between the calculated and experimental thermodynamic properties and cold compression curves of TATB crystal. Also, they calculated the full set of the second-order elastic constants at zero pressure. However, involvement of the experimental data does not allow the properties of other energetic materials to be calculated directly from these force fields without their re-parameterization.

Valenzano *et al.*[13] reported some second-order elastic constants for TATB at zero pressure. They were obtained with density functional theory in the Gaussian basis set with an *a posteriori* account of dispersion forces. The volume of the unit cell, in contrast to this work, was fixed at the experimental ambient temperature value, though lattice parameters and atomic positions were allowed to relax. The relation of C_{11} to C_{33} leads to the conclusion that stiffness of TATB crystal along the *a* and *b* axes is about four times larger than in the *c* direction.

In general, there are 21 non-zero elastic constants for crystals with the $P\bar{1}$ triclinic space group. This circumstance considerably complicates the calculation of C_{ij} in such crystals. For the calculation of the second-order elastic constants at zero and non-zero pressures, we used a theoretical approach based on total energy variation under certain deformations ("energy-strain relations").[35,36] Deformed structures were generated in a semiautomatic mode using the `ElaStic` set of scripts.[37]

For each deformation, one needs to generate a set of structures in which the small parameter η characterizing the degree of this deformation takes values from $-\eta$ to $+\eta$. We used 25 structures for each deformation and each pressure value. The obtained set of points can further be approximated by a polynomial dependence. For these calculations, we also used `ElaStic`. The determination of the polynomial parameters (maximal deformation for approximation and the polynomial degree) in each case was carried out manually. Mostly, we used 4- and 6-order polynomials. The minimal value of total energy deviation and convergence to a constant as the deformation range reduced were the criteria of optimal polynomial parameters.

As a result, a set of polynomial equations linking total energy and deformation were obtained. The coefficients at a quadratic term, α, are functionally linked to the elastic constants and applied pressure, P (see Ref. 36 for additional information)

$$\frac{2\alpha}{V_0} = f(C_{ij}, P), \tag{3}$$

where V_0 is the equilibrium cell volume at given pressure. It should be noted that the described method of calculation of elastic constants is quite general and can be extended to other molecular crystals.

Thus, twenty one curves of energy dependence on applied deformation for each pressure were obtained. The approximation polynomial parameters were then passed to `ElaStic` to compute C_{ij}. For non-zero pressures, the values of C_{ij} should be corrected. In Voigt notation,[38] transition equations are written as

$$\begin{aligned} &\tilde{C}_{ii} = C_{ii} - P, \quad i = 1,2,...,6; \\ &\tilde{C}_{12} = C_{12} + P, \quad \tilde{C}_{13} = C_{13} + P, \quad \tilde{C}_{23} = C_{23} + P; \\ &\tilde{C}_{ij} = C_{ij}, \quad i = 1,2,3; \quad j = 4,5,6; \\ &\tilde{C}_{45} = C_{45}, \quad \tilde{C}_{46} = C_{46}, \quad \tilde{C}_{56} = C_{56}. \end{aligned} \tag{4}$$

The zero-pressure elastic constants of TATB crystal together with the values calculated in Refs. 13 and 34 are listed in Table III. The agreement between three works is reasonable. On the whole, the values of elastic constants are found to agree better with those obtained by Bedrov *et al.* using polarizable force field in comparison with non-polarizable force field data. It can be speculated that the further improvement and complication of classical force fields will lead to a better agreement with our values obtained from the first principles.

As diamond anvil experiments for TATB are only available up to 13.0 GPa and the measurements of elastic properties are associated with additional difficulties, for the calculation of elastic constants at finite pressures we chose three points in the region of 0–13 GPa that can, in principle, be tested experimentally. The corrected values of elastic

TABLE III. Elastic constants of TATB crystal at the zero pressure. The results of Ref. 34 are given both for dipole polarizable and nonpolarizable force fields.

Elastic constant	This work	Classical MD (polarizable FF) (Ref. 34)	Classical MD (nonpolarizable FF) (Ref. 34)	*Ab initio* values (Ref. 13)
C_{11}	83.2	65.7 ± 0.5	57.5 ± 0.5	78.4
C_{22}	78.3	62.0 ± 1.0	58.0 ± 1.0	
C_{33}	18.9	18.3 ± 0.5	17.0 ± 0.5	19.7
C_{44}	1.7	1.4 ± 0.3	1.0 ± 0.3	0.9
C_{55}	1.5	0.68 ± 0.06	0.6 ± 0.2	
C_{66}	30.0	21.6 ± 0.7	20.3 ± 0.8	29.7
C_{12}	21.9	18.5 ± 0.5	16.2 ± 0.7	16.8
C_{13}	−2.4	4.0 ± 2.0	3.2 ± 0.5	0.8
C_{23}	−0.3	5.0 ± 1.0	5.7 ± 0.6	
C_{14}	−0.8	−0.2 ± 0.3	0.1 ± 0.1	
C_{15}	−0.6	−1.0 ± 0.1	−0.9 ± 0.2	
C_{16}	2.9	1.0 ± 1.0	0.0 ± 1.0	
C_{24}	0.1	0.6 ± 0.2	0.6 ± 0.2	
C_{25}	−0.4	−0.5 ± 0.2	−0.5 ± 0.3	
C_{26}	2.5	1.0 ± 1.0	2.0 ± 0.8	
C_{34}	−0.6	0.2 ± 0.3	−0.1 ± 0.4	
C_{35}	−0.5	−0.4 ± 0.1	−0.3 ± 0.2	
C_{36}	0.1	−0.4 ± 0.7	−1.0 ± 0.5	
C_{45}	0.0	0.1 ± 0.2	0.01 ± 0.04	
C_{46}	−0.3	0.3 ± 0.2	−0.5 ± 0.1	
C_{56}	0.6	0.4 ± 0.1	0.1 ± 0.1	

TABLE IV. Elastic constants of TATB at the pressures 2, 5, and 10 GPa.

Elastic constant	2 GPa	5 GPa	10 GPa
$\tilde{C}_{11}$	121.1	177.3	257.0
$\tilde{C}_{22}$	115.3	170.9	249.5
$\tilde{C}_{33}$	45.7	80.7	130.5
$\tilde{C}_{44}$	4.9	9.2	15.2
$\tilde{C}_{55}$	4.3	8.1	13.3
$\tilde{C}_{66}$	44.2	63.5	90.0
$\tilde{C}_{12}$	32.4	50.7	77.6
$\tilde{C}_{13}$	4.5	14.0	26.6
$\tilde{C}_{23}$	7.2	16.1	29.3
C_{14}	0.2	1.3	1.7
C_{15}	0.0	1.5	2.0
C_{16}	0.7	0.4	−0.4
C_{24}	0.5	0.2	0.0
C_{25}	0.2	0.2	0.5
C_{26}	1.5	−0.7	−0.4
C_{34}	−1.0	−1.2	−1.4
C_{35}	0.3	0.8	1.1
C_{36}	1.0	0.5	0.1
C_{45}	0.1	0.4	0.4
C_{46}	0.1	0.2	0.4
C_{56}	1.0	1.2	1.8

constants for the pressures 2, 5, and 10 GPa are given in Table IV.

It should be noted that the ratio of the averaged values of $\tilde{C}_{11}$ and $\tilde{C}_{22}$ to $\tilde{C}_{33}$ sharply decreases as pressure grows. At zero pressure it equals 4.3:1 (in accordance with the results obtained from first principles in Ref. 13), at 2 GPa it is 2.6:1, and at 10 GPa it is only 1.9:1. Thus, the rapid hardening of TATB crystal along the c crystallographic axis with the growth of pressure is observed.

From the corrected elastic constants, the bulk, B, and shear, G, moduli can be obtained. Following Voigt,[39] their values are calculated using the stiffness matrix $\mathbf{C}$ and within the Reuss[40] approach the compliance matrix $\mathbf{S}$ (which is obtained by the inversion of $\mathbf{C}$) is used

$$B_V = \frac{1}{9}\left[\left(\tilde{C}_{11}+\tilde{C}_{22}+\tilde{C}_{33}\right)+2\left(\tilde{C}_{12}+\tilde{C}_{13}+\tilde{C}_{23}\right)\right], \quad (5)$$

$$B_R = \left[\left(\tilde{S}_{11}+\tilde{S}_{22}+\tilde{S}_{33}\right)+2\left(\tilde{S}_{12}+\tilde{S}_{13}+\tilde{S}_{23}\right)\right]^{-1}, \quad (6)$$

$$G_V = \frac{1}{15}\left[\left(\tilde{C}_{11}+\tilde{C}_{22}+\tilde{C}_{33}\right)-\left(\tilde{C}_{12}+\tilde{C}_{13}+\tilde{C}_{23}\right)+3\left(\tilde{C}_{44}+\tilde{C}_{55}+\tilde{C}_{66}\right)\right], \quad (7)$$

$$G_R = 15\left[4\left(\tilde{S}_{11}+\tilde{S}_{22}+\tilde{S}_{33}\right)-4\left(\tilde{S}_{12}+\tilde{S}_{13}+\tilde{S}_{23}\right)+3\left(\tilde{S}_{44}+\tilde{S}_{55}+\tilde{S}_{66}\right)\right]^{-1}. \quad (8)$$

Using the Voigt and Reuss moduli as upper and lower bound, correspondingly,[41,42] the bulk, B, and the shear, G, moduli for the polycrystal were obtained by averaging. Then, from the values of B and G, the Young modulus, E, and the Poisson ratio, ν, were calculated using well known relations (see, for example, Ref. 43).

The values of elastic moduli calculated from elastic constants at pressures 0, 2, 5, and 10 GPa are presented in Table V. The zero-pressure values are in a good agreement with the results obtained using classical molecular dynamics with a dipole polarizable force field (18.15 GPa for the bulk modulus and 7.3 GPa for the shear modulus). Moreover, the bulk modulus agrees well with the estimation obtained by fitting the calculated cold curve with the isothermal equations of state in the form of Vinet (18.0 ± 0.9 GPa) and Birch-Murnaghan (17.0 ± 1.2 GPa).

TABLE V. Elastic moduli (GPa) and the Poisson ratio values at 0, 2, 5, and 10 GPa.

Elastic modulus	0 GPa	2 GPa	5 GPa	10 GPa
B_V	24.31	41.14	65.61	100.44
G_V	17.39	26.55	39.37	57.27
B_R	12.90	31.08	54.15	86.57
G_R	3.51	9.58	17.36	27.99
B	18.61	36.11	59.88	93.51
G	10.45	18.06	28.36	42.63
E	26.40	46.45	73.49	111.02
ν	0.2635	0.2856	0.2955	0.3021

B. Sound speeds

Longitudinal, C_L, shear, C_S, and bulk, C_{bulk}, sound speeds were calculated from the elastic moduli[43] which, in turn, were obtained from the elastic constants $\tilde{C}_{ij}$

$$C_L = \sqrt{\frac{E(1-\nu)}{\rho(1+\nu)(1-2\nu)}}; \quad C_S = \sqrt{\frac{E}{2\rho(1+\nu)}}; \quad C_{\text{bulk}} = \sqrt{C_L^2 - 4/3C_S^2}, \quad (9)$$

where ρ is density (Table II). At zero temperature, we can directly use the elastic moduli calculated above (Table VI). The bulk sound speed at zero pressure can be evaluated from the coefficient B of the Vinet and Murnaghan-Birch equations of state, which corresponds to the bulk elastic modulus, and experimentally determined density of TATB crystal[4] with the simple relation $C_{\text{bulk}} = \sqrt{B/\rho}$. The results of this estimation are given in Table VII. For the experimental data, we used density 1.937 g/cm^3 from Ref. 4, and for our

TABLE VI. The speeds of sound (in km/s) determined from the bulk moduli.

Sound speed	0 GPa	2 GPa	5 GPa	10 GPa
C_L	4.05	5.26	6.46	7.73
C_S	2.30	2.88	3.48	4.11
C_{bulk}	3.06	4.07	5.06	6.09

TABLE VII. The bulk sound speed (in km/s) at zero pressure from the equations of state.

	C_{bulk}		
Equation of state	Olinger and Cady[4]	Stevens *et al.*[23]	This work
Vinet	2.89	3.00	3.01
3rd order Birch-Murnaghan	2.89	2.96	2.93

calculation we used density at zero pressure and temperature (1.983 g/cm^3). The calculated and experimental values listed in Tables VI and VII are in a good agreement. Values in Table VI show that the growth of sound speed is gradually decreases as pressure grows. The bulk sound speed doubles near 10 GPa. We can also compare C_{bulk} at zero pressure with experimentally available data on shock velocity, U_S, extrapolated to zero particle velocity, u_p. For example, Gustavsen *et al.*[44,45] obtained the shock adiabat of TATB-based formulation PBX 9502 (95% TATB and 5% Kel-F 800 binder) both for room temperature and for −55 °C. We approximated their data by a linear dependence and obtained the value of C_{bulk} to be equal to 3.05 km/s with the correlation coefficient $R = 0.989$. It supports our estimations on sound speeds in TATB, at least determined at zero pressure.

IV. CONCLUSION

We have considered the effects of pressure on some thermodynamic, elastic, and acoustic properties of TATB crystal at zero temperature. It is shown that the use of dispersion corrections for this purpose is mandatory and that the classical DFT approaches give erroneous equilibrium cell properties and fails to estimate their relative changes under external pressure. Then, we discovered that the optimal calculation parameters that ensure total energy convergence at the level 0.1 mRy/atom are relatively strict: at least 60 Ry (about 800 eV) for the plane wave basis set size and at least 8 *k*-points in reciprocal space at zero pressure. Using density functional theory with dispersion corrections, we found the unit cell parameters and the changes that take place with the unit cell and TATB molecules at the compression up to 50 GPa, which agree well with available experimental data. It is shown that the most compressible covalent bond in TATB is C-NO_2. As pressure grows, the intermolecular distance H···H decreases steeper than the distances N···C and H···C. It means that molecules in adjacent layers are bended towards each other.

Although elastic constants are of great importance for the understanding of mechanical properties in crystals, their full set for TATB has not yet been determined experimentally or calculated from first principles. In this work, we for the first time calculated the full set of elastic constants and elastic moduli for TATB crystal at zero and some non-zero pressures using *ab initio* methods. The described method of elastic constants calculation is quite general and can safely be extended to other molecular crystals. In the majority of cases, the values of elastic constants are found to be in a better agreement with the ones obtained in Ref. 34 using polarizable force field in comparison with non-polarizable force field data. This suggests that further improvement and complication of classical force fields will help to make differences between the values of elastic constants yet smaller. The comparison of calculated and experimental values for the bulk moduli and sound speeds shows that the data obtained with the dispersion corrected density functional theory method can be used to predict the elastic and acoustic properties of the TATB molecular crystal.

[1] I. Ledoux, J. Zyss, J. S. Siegel, J. Brienne, and J.-M. Lehn, Chem. Phys. Lett. **172**, 440 (1990).
[2] I. G. Voight-Martin, G. Li, A. Yakimanski, G. Schultz, and J. J. Wolff, J. Am. Chem. Soc. **118**, 12830 (1996).
[3] S. F. Son, B. W. Asay, B. F. Henson, R. K. Sander, A. N. Ali, P. M. Zielinski, D. S. Philips, R. B. Schwarz, and C. B. Skidmore, J. Phys. Chem. B **103**, 5434 (1999).
[4] H. H. Cady and A. C. Larson, Acta Cryst. **18**, 485 (1965).
[5] A. D. Becke, J. Chem. Phys. **140**, 18A301 (2014).
[6] E. F. C. Byrd and B. M. Rice, J. Phys. Chem. C **111**, 2787 (2007).
[7] J. P. Perdew, in *Electronic Structures of Solids'91*, edited by P. Ziesche and H. Eschrig (Akademie-Verlag, Berlin, 1991).
[8] J. P. Perdew, K. Burke, and M. Ernzerhof, Phys. Rev. Lett. **77**, 3865 (1996).
[9] S. Grimme, J. Comput. Chem. **27**, 1787 (2006).
[10] M. Budzevich, M. Conroy, A. Landerville, Y. Lin, I. Oleynik, and C. T. White, AIP Conf. Proc. **1195**, 545 (2009).
[11] M. M. Budzevich, A. C. Landerville, M. W. Conroy, Y. Lin, I. I. Oleynik, and C. T. White, J. Appl. Phys. **107**, 113524 (2010).
[12] D. C. Sorescu and B. M. Rice, J. Phys. Chem. C **114**, 6734 (2010).
[13] L. Valenzano, W. J. Slough, and W. Perger, AIP Conf. Proc. **1426**, 1191 (2012).
[14] I. A. Fedorov and Yu. N. Zhuravlev, Chem. Phys. **436–437**, 1 (2014).
[15] P. Giannozzi, S. Baroni, N. Bonini, M. Calandra, R. Car, C. Cavazzoni, D. Ceresoli, G. L. Chiarotti, M. Cococcioni, I. Dabo, A. Dal Corso, S. Fabris, G. Fratesi, S. de Gironcoli, R. Gebauer, U. Gerstmann, C. Gougoussis, A. Kokalj, M. Lazzeri, L. Martin-Samos, N. Marzari, F. Mauri, R. Mazzarello, S. Paolini, A. Pasquarello, L. Paulatto, C. Sbraccia, S. Scandolo, G. Sclauzero, A. P. Seitsonen, A. Smogunov, P. Umari, and R. M. Wentzcovitch, J. Phys.: Condens. Matter **21**, 395502 (2009).
[16] D. E. Taylor, J. Phys. Chem. A **117**, 3507 (2013).
[17] D. Vanderbilt, Phys. Rev. B **41**, 7892 (1990).
[18] N. Troullier and J. L. Martins, Phys. Rev. B **43**, 1993 (1991).
[19] N. Troullier and J. L. Martins, Phys. Rev. B **43**, 8861 (1991).
[20] P. Pulay, Mol. Phys. **17**, 197 (1969).
[21] P. Pulay, Adv. Chem. Phys. **69**, 241 (1987).
[22] D. Marx and J. Hutter, *Ab Initio Molecular Dynamics: Basic Theory and Advanced Methods* (Cambridge University Press, Cambridge, 2009).
[23] L. L. Stevens, N. Velisavljevic, D. E. Hooks, and D. M. Dattelbaum, Propellants, Explos. Pyrotech. **33**, 286 (2008).
[24] B. Olinger and H. Cady, in *Proceedings of Sixth International Symposium on Detonation, Coronado, California, USA, August 24–27, 1976*, p. 700 (unpublished).
[25] P. Vinet, J. R. Smith, J. Ferrante, and J. H. Rose, Phys. Rev. B **35**, 1945 (1987).
[26] F. Birch, Phys. Rev. **71**, 809 (1947).
[27] K. K. Baldridge and J. S. Siegel, J. Am. Chem. Soc. **115**, 10782 (1993).
[28] A. J. Davidson, R. Dias, D. Dattelbaum, and C. Yoo, J. Chem. Phys. **135**, 174507 (2011).
[29] M. Pravica, B. Yulga, Z. X. Liu, and O. Tschauner, Phys. Rev. B **76**, 064102 (2007).
[30] M. Pravica, B. Yulga, S. Tkachev, and Z. X. Liu, J. Phys. Chem. A **113**, 9133 (2009).
[31] M. R. Manaa and L. E. Fried, J. Phys. Chem. C **116**, 2116 (2011).
[32] O. Ojeda and T. Çağin, J. Phys. Chem. B **115**, 12085 (2011).
[33] R. F. W. Bader, *Atoms in Molecules—A Quantum Theory* (Oxford University Press, Oxford, 1990).
[34] D. Bedrov, O. Borodin, G. D. Smith, T. D. Sewell, D. M. Dattelbaum, and L. L. Stevens, J. Chem. Phys. **131**, 224703 (2009).
[35] Y. Le Page and P. Saxe, Phys. Rev. B **63**, 174103 (2001).
[36] G. V. Sin'ko and N. A. Smirnov, J. Phys.: Condens. Matter **14**, 6989 (2002).
[37] R. Golesorkhtabar, P. Pavone, J. Spitaler, P. Puschnig, and C. Draxl, Comput. Phys. Commun. **184**, 1861 (2013).
[38] M. I. Katsnelson and A. V. Trefilov, *Dynamics and Thermodynamics of a Crystal Lattice* (IzdAT, Moscow, 2002) (in Russian).
[39] W. Voigt, *Lehrbuch der Kristallphysik* (B.G. Teubner, 1928), p. 962.
[40] A. Reuss, Z. Angew. Math. Mech. **9**, 49 (1929).
[41] R. Hill, Proc. Phys. Soc. London, Sect. A **65**, 349 (1952).
[42] R. Hill, J. Mech. Phys. Solids **11**, 357 (1963).
[43] L. D. Landau and E. M. Lifshitz, *Theoretical Physics*, Theory of Elasticity Vol. VII (Nauka, Moscow, 1987) (in Russian).
[44] R. L. Gustavsen, S. A. Sheffield, and R. R. Alcon, J. Appl. Phys. **99**, 114907 (2006).
[45] R. L. Gustavsen, R. J. Gehr, S. M. Bucholtz, R. R. Alcon, and B. D. Bartram, J. Appl. Phys. **112**, 074909 (2012).